LA-UR -80-224

TITLE: THERMOMECHANICAL MODELS OF THE RIO GRANDE RIFT

AUTHOR(S): R. J. Bridwell and C. A. Anderson

SUBMITTED TO: NATO ASI "The Mechanisms of Continental Drift and Plate Tectonics," S. K. Runcorn, Ed., Newcastle-upon-Tyne, England

MASTER

University of California

LOS ALAMOS SCIENTIFIC LABORATORY
Post Office Box 1663 Los Alamos, New Mexico 87545
An Affirmative Action/Equal Opportunity Employer

Form No. 836 R3
St. No. 2629
12/78

UNITED STATES
DEPARTMENT OF ENERGY
CONTRACT W-7405-ENG. 36

THERMOMECHANICAL MODELS OF THE RIO GRANDE RIFT

by

R. J. Bridwell

Geoscience Division

and

C. A. Anderson

Energy Division

Los Alamos Scientific Laboratory

University of California

Los Alamos, New Mexico 87545

for

NATO Advanced Study Institute

"The Mechanism of Continental Drift and Plate Tectonics"

School of Physics, The University, Newcastle-upon-Tyne

January, 1980

ABSTRACT

Fully two-dimensional, coupled thermomechanical solutions of a continental rift and platform are used to model the crust and mantle structure of a hot, buoyant mantle diapir beneath the Rio Grande rift. The thermomechanical model includes both linear and nonlinear laws of the Weertman type relating shear stress and creep strain rate, viscosity which depends on temperature and pressure, and activation energy, temperature dependent thermal conductivity, temperature dependent coefficient of thermal expansion, the Boussinesq approximation for thermal buoyancy, material convection using a stress rate that is invariant to rigid rotations, an elastically deformable crust, and a free surface. A priori, we require a temperature T_0 at the free surface, volumetric heating by radioactive heat generation, and influx of heat q^∞ at great depth. In addition we specify thermal and mechanical properties using a Newtonian crust and non Newtonian mantle. The model determines the free surface velocities, solid state flow field in the mantle, and viscosity structure of lithosphere and asthenosphere. Geologic data including an Eocene erosion surface as a horizontal datum, recent geologic evidence of regional uplift in late Miocene-to-Recent-time (<15 m.y.), regionally averaged topography, the temporal and spatial nature of Cenozoic volcanism, and geotherms from mantle xenoliths to asthenospheric depths provide fundamental constraints on the model. We simulate regional topography and crustal heat flow. A suite of symmetric models, assumes continental geotherms on the right and the successively increasing rift geotherms on the left. These models predict an asthenospheric flow field which transfers cold material laterally toward the rift at >300 km, hot, buoyant material ~200 km wide which ascends vertically at rates of 1 km/m.y. between 175-325 km, and spreads laterally away from the

rift at the base of the lithosphere. Crustal spreading rates are similar to uplift rates. The lithosphere acts as stiff, elastic 'cap', damping upward motion through decreased velocities of 1 km/10 m.y. and spreading uplift laterally. A parameter study varying material coefficients for the Weertman flow law

$$\dot{\varepsilon} = Ae^{-(E^* + PV^*)/RT_\tau n}$$

suggests best fit values of A = 3.4 kbars^{-n}, n = 3, E* = 110 kcal/mol, and V* = 17 cm^3/mol for mantle materials provide asthenospheric viscosities of $\sim 10^{22}$ -10^{23} poise. Similar studies predict crustal viscosities of $\sim 10^{25}$ poise. The buoyant process of mantle flow narrows and concentrates heat transport beneath the rift, increases upward velocity, and broadly arches the lithosphere.

INTRODUCTION

Genesis of a continental rift is closely tied to understanding its thermal history. Interactions of convective heat and mass with materials of the lithosphere cause thinning, magma genesis, uplift, an extensional stress state, normal faulting, and ultimately, extrusion of surficial volcanics.

Various static models have been proposed along the Rio Grande rift to discuss the geometry of the continental lithosphere. Decker and Smithson (1975) utilized Bouguer gravity data to suggest a low density sill at depths of 31 km beneath the southern rift. Surface heat flows >2.5 HFU, (Reiter et al., 1975)(1 HFU = μcal/cm^{2}S = 41.8 mW/m^2) provided a geotherm which intersects typical mantle solidi at depths of 25 to 31 km in a conductive lithosphere (Decker and Smithson, 1975). Ramberg, et al. (1978)

models suggest crustal attenuation may be accounted for by extension and partial melting in the southern rift (Cook et al., 1979). In the northern rift, a mass deficiency of ~0.1 g/cm^3 for the upper mantle is caused by a mantle diapir with high temperatures beneath the rift (Bridwell, 1976); a second paper, using steady-state conductive models and estimates of the geotherm from surface heat flow and a conductive lithosphere predicted a viscosity minima of 10^{20} poises beneath the rift with an associated increase in effective stress gradients in the crust and upper mantle beneath the rift (Bridwell, 1978a). The physical state of the continental lithosphere has been characterized as having nigh temperatures, low density, low viscosity, and high effective stress gradients beneath the rift at depths of 40 to 80 km (Bridwell, 1978b).

In this paper, we treat the dynamic aspects of lithospheric thinning by providing coupled thermomechanical models, using the finite element technique, of a continental rift and platform. A model is presented to evaluate the dynamic process of uplift and continental rifting. This model uses nonlinear flow laws, thermally-dependent material properties, thermal gradients varying from continental rift to platform, and the Boussinesq approximation of temperature dependent buoyancy to drive the uplift. Constraints for new dynamic models are based on geologic and geophysical data such as uplift, uplift rates, Cenozoic volcanism in New Mexico, crust and mantle geotherms from rift and platform, and present surface heat flow. Uplift rates and magnitudes for northern New Mexico are calculated from regionally averaged topography, paleobotanical data, and stratigraphic relations. Crust and mantle geotherms are determined petrologically using natural xenoliths which provide P, T data. A suite of temperature conditions is analyzed to show the spectrum of thermomechanical behavior

during development of a continental rift. This dynamic study is the first to consider the deformable lithosphere and convective flow in the underlying asthenosphere for the Rio Grande rift.

REGIONAL UPLIFT

Modeling regional uplift requires knowledge of an initial undeformed structural datum, the amount of uplift, and its duration. A number of geologic events, such as formation of the late Eocene erosional surface of the southwestern United States, deposition of widespread Miocene basins, temporal nature of magmatism and volcanism including a mid-Miocene lull in volcanism, duration of uplift, and present elevations, bear directly on the mechanism of continental rifting.

The post-Laramide, late Eocene erosion surface of the southern Rocky Mountains and Datil-Mogollon volcanic field of west-central New Mexico is a fundamental regional structural datum (Epis and Chapin, 1975). The late Eocene erosion surface had initially low relief of ~0.5-0.9 km ~35 m.y. ago. Regional extension began ~29 m.y. ago (Chapin and Seager, 1975), with little uplift and development of broad basins in Miocene time along the length of the rift from 26-10 m.y. ago (Chapin, personal communication, 1979). Present uplift occurs over a broad region in New Mexico. Figure 1 shows regionally averaged topography ranging in elevation from ~1.2-2.4 km (Aiken et al., 1978). The majority of the Rio Grande rift occurs in regions showing topography of 1.5-2.1 km. If the Eocene erosion surface was at elevations of 0.5-0.7 km (Epis and Chapin, 1975; Axelrod and Bailey, 1976), then relative regional motion would be 1-1.4 km. Since geologic relations in latest Miocene time ~10 m.y. ago date the onset of motion, regional uplift also occurred with a relative velocity of 1-1.4 km/10 m.y.

CENOZOIC VOLCANISM AND THERMAL EVOLUTION OF RIFTING

Thermal evolution of the Rio Grande rift is indicated by the spatial, temporal, and chemical nature of volcanic and plutonic rocks. Chapin and Seager (1975) documented 161 K/Ar and fission track dates of late Eocene to Holocene age in New Mexico as shown in Figure 2a. There are clearly two temporal maxima at 40-20 m.y. and 15-1 m.y. ago separated by the Miocene lull. Taken at face value, this would suggest two thermal pulses within the lithosphere since formation of the late Eocene erosion surface.

Application of a spatial filter reduces the complexity of the thermal pulses. Most of the rocks shown in Figure 2a in the time span 40-20 m.y. ago are from the Datil-Mogollon volcanic pile in southwestern New Mexico although the most of the stocks and dikes are associated with the Rio Grande rift (Chapin, personal communication, 1979). Hence, although some volcanism is associated with the rift prior to the Miocene lull, it is small in volume compared to the basaltic volcanism of late Miocene to recent time (e.g., Baldridge, et al, 1980). Note in Figure 2b the regional distribution of volcanism from Colorado to central New Mexico.

The presence and age of basaltic volcanism of <10 m.y. age indicates melting and magma formation in the lowermost crust and uppermost mantle. Although basaltic volcanism (basaltic andesites of Chapin and Seager, 1975) occurred prior to the Miocene lull, only small volumes of rocks occur in the Espanola, Albuquerque, southern San Luis, and Arkansas basins. The relatively voluminous fields of the Taos Plateau, Jemez Mountains, Cerros del Rio, Mt. Taylor, Cat Hills, Wind Mesa, and others followed the Miocene lull. It is tempting to postulate thermal changes such as mass flux in the lithosphere and increased surface heat flow based on the simple function shown in figure 2c.

THERMAL GRADIENTS OF A CONTINENTAL RIFT

A continental platform geotherm has been determined for the Colorado Plateau to depths of several hundred km by McGetchin and Silver (1972), shown in Figure 3. The continental rift geotherm, shown in Figure 3, is a composite geotherm utilizing geobarometry from crust and mantle xenoliths principally at Kilbourne Hole Maar, New Mexico. Geobarometry data are discussed by Bridwell and Anderson (1980). The crustal segment has a slope of 32°C/km and agrees well with an average surface heat flow of 2.5 HFU determined by Decker and Smithson (1975) as shown by Padovani and Carter (1977). The asthenosphere is modeled as a subsolidus regime beneath the continent. Since temperatures beneath the continental rift are excessive at relatively shallow depths in the presence of Mercier's (1977) 4°C/km gradient to 100 km, we assume a superadiabatic gradient to 200 km and an adiabatic gradient (0.5°C/km) for the rift geotherm below 200 km. This results in a temperature increase of ~100°C relative to the continental geotherm at the 400 km olivine-spinel phase transition.

THERMOMECHANICAL MODEL

Recent work has produced one-dimensional models of the coupled thermomechanical structure of oceanic and continental lithospheres (Schubert and Turcotte, 1972; Froidevaux and Schubert, 1975; Schubert, et al., 1976). A quasi-two dimensional model of oceanic mantle circulation with partial shallow return flow considers plate stresses (Schubert, et al., 1978). In this paper, we consider the fully two-dimensional, coupled thermomechanical behavior of a continental rift and platform. The thermal and mechanical structure of a continental lithosphere and asthenosphere are coupled via

several effects; the dependence of viscosity on temperature, temperature dependent material properties, and the Boussinesq approximation of density change due to temperature.

A conceptual two-dimensional model initial conditions for a continental rift and platform in plane strain symmetric about the ordinate, is shown in Figure 4. The relatively cool continental platform on the right has negative buoyancy whereas the less-dense relatively hot continental rift on the left has positive buoyancy. The relative positive buoyancy causes asthenospheric flow toward the rift at depth, hot buoyant upward diapiric motion beneath the rift, and lateral shear flow outward beneath the crust associated with uplift of the shoulder of the rift. In Figure 4, we list thermal and mechanical quantities required by our models.

At the surface, we specify the temperature $T = T_o$. At great depth (400 km), we specify the mantle flux q_∞. Adiabatic conditions are specified on the vertical boundaries. The heat generation H and the thermal conductivity K vary within each layer. The densities are shown for each layer. Mechanical boundary conditions consist of no flow across either the 400 km olivine phase transition or the vertical boundaries. The upper two layers are lithosphere with crust and upper mantle whereas the lower layer is asthenosphere. The unknowns of temperature, effective viscosity, heat flow, and topography are provided by model calculations.

Our model includes the following features:

(1) linear or nonlinear flow law relating shear stress, shear stress rate, and strain rate, Eq. 1,

(2) temperature- and pressure-dependent viscosity,

(3) temperature-dependent thermal conductivity,

(4) temperature-dependent bulk coefficient of thermal expansion

(5) temperature-dependent density through Boussinesq approximation for buoyancy, Eq. 4,

(6) material convection using a frame invariant stress rate,

(7) a free surface, and

(8) an elastically deformable crust.

MATHEMATICAL FORMULATION

The equations governing the thermomechanical behavior of a continental rift and platform are the constitutive law and the two-dimensional equations of energy conservation and stress equilibrium (Anderson and Bridwell, 1980).

The constitutive law used for describing the mechanical behavior of the model is of the form

$$\dot{\epsilon}_{ij} = \frac{(1+\nu)}{E} \overset{\nabla}{\sigma}_{ij} - \frac{\nu}{E} \delta_{ij} \overset{\nabla}{\sigma}_{kk} + \frac{1}{\eta} s_{ij} \qquad (1)$$

where $\dot{\epsilon}_{ij}$ is the strain rate tensor, $\overset{\nabla}{\sigma}_{ij}$ is a frame invariant stress rate tensor (Prager, 1961), s_{ij} is the stress deviator tensor, ν and E are Poisson's ratio and Young's modulus respectively, and η is the material viscosity. In Eq. (1) the indicial notation is applied (i, j = 1,2,3) with repeated index implying a summation and with δ_{ij} = 0, i≠j or 1, i=j being the Kronecker delta. The viscosity is determined by the state of stress and the temperature through an equation of the Weertman form,

$$\eta = \frac{e^{(E^* + pV^*)/RT}}{A_T^{n-1}}, \qquad (2)$$

where A and n are experimentally determined constants, E* and V* are activation energy and volume respectively, P is the mean stress, R is the

universal gas constant, T is the absolute temperature, and τ is the effective stress given by

$$\tau = (1/2\ s_{ij}\ s_{ij})^{1/2} . \tag{3}$$

The Boussinesq approximation assumes that density variations due to changes in temperature occur in the gravitational or buoyancy term of the equations of motion. All other variations in density are neglected. The approximation is justified if variations are small compared with the mean density of the rock. Dynamically important variations in density, ignoring the effect of phase changes, can be written as a function of temperature alone

$$\rho = \rho_0[1 + \alpha\ (T_r - T)] \tag{4}$$

where ρ_0 is mean density at reference temperature T_r, T is the temperature of element, and α bulk or volume coefficient of thermal expansion.

The energy equation is

$$\rho C_p \frac{\partial T}{\partial t} = H + K \frac{\partial^2 T}{\partial x^2} + \sigma_{ij}\ \dot{\varepsilon}_{ij} \tag{5}$$

where C_p is heat capacity, H is heat generation, K is thermal conductivity, and σ_{ij} and $\dot{\varepsilon}_{ij}$ are the stress and strain-rate tensors. Again, repeated index cycles summation over that index. The first term represents material convection, the second heat generation, the third heat conduction, and the last term is shear strain heating.

Equation (1) - (4) together with the equilibrium equations, the strain rate-velocity relations, and the definition of the frame invariant stress

rate (Prager, 1961) constitute the physical equations of the thermo-mechanical model. The equations are discretized using the finite element method and a numerically stable time stepping algorithm is used to advance the physical quantities stress, temperature, and velocity from an initially specified equilibrium stress and temperature state. Details are given in Anderson and Bridwell (1980).

THERMOMECHANICAL MATERIAL PROPERTIES

The behavior of the equations of motion depends on such material parameters as thermal conductivity, heat capacity, density, bulk coefficient of thermal expansion, elastic modulus, and non-Newtonian rheological coefficients. Each will be discussed in detail below.

Thermal conductivities have been measured in surficial granitic rocks. Of 100 values, the average is 2.3 W/m°C (Blackwell, 1971). No temperature variation is known. For upper mantle rocks, such as pyrolite or spinel lherzolite, Schatz and Simmons (1972) found a temperature dependence in the range 325-1625°C for polycrystalline forsterite-rich olivines. In our model, conductivities of the crust are from measured values cited by Blackwell (1971) and conductivities of the mantle are from Schatz and Simmons (1972). The heat capacity is assumed constant at ~1250 J/kg°C.

Densities are based on seismic profiles using the well-known relation between P-wave velocities and density. Densities are 2.7 g/cm^3 for th upper crust, 2.85 g/cm^3 for the lower crust, 3.3 g/cm^3 for the cold upper mantle, and 3.2 g/cm^3 for the low velocity zone in the mantle (Olsen, et al, 1979).

The bulk or volume coefficient of thermal expansion varies linearly with temperature. Several minerals are shown to increase their thermal

expansion linearly to 800°C (Skinner, 1966). We use crust and mantle thermal expansions from Skinner extrapolated to 1400°C because of the clear separation in α's for feldspars and olivine/pyroxenes. For feldspars of Ab_{56}-An_{44}, α ranges from 12-24 X $10^{-6}°C^{-1}$ whereas for olivines and pyroxenes α ranges from 26-40 X $10^{-6}°C^{-1}$.

Elastic moduli are chosen as a maximum of 1 Mb for crustal materials. Because of the stability criterion on time steps for the finite element method (Anderson and Bridwell, 1980) the elastic moduli are decreased as a function of temperature to values ~100 bars in regions at temperatures of 1400°C.

We assume that the creep law describes the Newtonian rheology of the crust and the non-Newtonian rheology of the mantle using for data that of high-temperature dislocation creep for dunite. For the Newtonian behavior, we choose a crustal viscosity which provides uplift rates of the free surface consistent with geologic data. The mantle rheology is non-Newtonian and we use an exponent of 3 on the effective stress. A suite of models was evaluated to predict values of E*, V*, and A for the rift. We eventually ran models described with E* = 110 kcal/mol, V* = 17 cm^3/mol, and A = 3.4 $Kbar^{-3}s^{-1}$. These values are consistent with experimental determinations of a "wet" dunite rheology as defined by Carter (1976). A recent determination of V* = 14 $\pm$ 3 cm^3/mol has been provided by Ross et al. (1979).

Lateral distribution of heat generation is assumed to give smooth temperature profiles ranging from low temperatures of a continental platform (600°C) to a successively increasing suite of high temperatures for a continental rift (>900°C) at the crust-mantle interface. The rift heat generation values from Table 1 are arbitrarily imposed 60 km from the left margin of the model, which, by symmetry, is the center of the rift.

TABLE 1 HEAT GENERATION TO PRODUCE THERMAL GRADIENTS

	Continental Rift		Continental Platform	
	Temperature at base of crust (40 km)			
	T=750°C q_s=71mW/m^2 =1.6 HFU	T=875°C q_s=88mW/m^2 =1.9 HFU	T=1000°C q_s=105mW/m^2 =2.5 HFU	T=600°C q_s=59mW/m^2 =1.4 HFU
Depth	HGU	HGU	HGU	HGU
0-10	2.1	2.1	2.1	2.1
10-40	1.18	1.37	1.65	0.88
40-100	0.23	0.20	0.186	0.025
100-200	0.095	0.073	0.069	0.025
200-400	0.026	0.021	0.013	0.025

1. A basal flux of 4.18 mW/m^2 is applied at a depth of 400 km.
2. 1 HGU = 10^{-13}cal/cm^{3}s = 0.418μ W/m^3.
3. q_s is surface heat flow where 1 HFU = 10^{-6}cal/cm^{2}s = 41.8 mW/m^2.

DISCUSSION OF RESULTS

The fully two-dimensional thermomechanical problem is formidable! The mathematical formulation provides temperature T, velocities u, v, and effective viscosity η as unknowns. We reduce some of the non-uniqueness by requiring vertical temperature profiles on the left-and-right-hand boundaries of the model to concur with Figure 3. We require the mantle viscosities to be determined by experimental measurements of dunite and regional geotherms although crustal viscosities are truly unknown. Since there is a range of measurements for flow coefficients of Eq. 2 as well as

a range of temperatures from Figure 3 which determine the viscosity and hence the velocity fields, we have conducted a number of numerical experiments to predict the viscosity. We have estimated the crustal viscosity by varying coefficients to obtain free surface velocities in quasi-steady-state flow which are consistent with geologic calculations of surface motions mentioned in the section on regional uplift. From these numerical experiments we present calculations of the viscosity, temperature, and velocity fields associated with formation of a continental rift.

A succession of thermal solutions was investigated to evaluate thermo mechanical behavior of continental rifts. Eq. 5 is solved at t_∞ with H specified in Table 1. These solutions produce temperature at the base of the crust of 750, 875, and 1000°C which are equivalent to heat flows of 1.6, 1.9, and 2.5 HFU respectively. Figure 5 shows isotherm contours of a rift model symmet c about the left ordinate. These thermal fields produce sufficient temperature differences to generate density changes (c.f. Eqs. 4 and 5) which drive buoyancy and create uplift. Density changes of less than 3% of regional values are sufficient to produce regional uplift.

Positive buoyancy associated with the temperature increase causes sub-solidus flow of crust and mantle materials from regions of relatively cool continent to hot rift. Free surface velocities are one of the unknowns of the numerical calculation. The vertical free surface motion at the center of the rift is shown in Figure 6 for surface heat flows having the range $1.6 < q_s < 2.5$ HFU. With time, velocity shows an initial rapid decay for ~8 m.y. followed by a 15-20 m.y. period where velocities are quasi-steady-state. The initial decay represents relaxation from the estimated elastic pre-stress state to the steady-state creep flow behavior.

We shall use flow velocities from the model for 8<t<25 m.y. for further discussions of steady-state creep and formation of continental rifts.

Although temperatures at the base of the crust vary considerably, vertical crustal velocities from Figure 6 for t > 8 m.y. fall in a relatively narrow band of 0.5-1.3 km/10 m.y. Figure 7 is a plot of vertical velocity versus depth for the symmetric centerline of the rift model. Velocities of the hot buoyant mantle diapir are ~1.2 km/m.y. An explanation for the variations in relative velocities lies in the differing behavior of the lithosphere and asthenosphere. The lithosphere is capped by a elastic crust with large temperature changes, yet which has only limited ability to creep. The upper mantle and asthenosphere are composed of mantle materials whose creep behavior is quite sensitive to increased temperature although these temperature changes are smaller. The lithosphere moves rather slowly, regardless of the surface heat flow, only showing a small increase in velocity with increasing temperature. In effect, it tends to damp out motions of the hot buoyant asthenosphere. In contrast, the buoyant asthenosphere beneath the rift moves 10 times faster, convecting heat and mass upward.

Horizontal motion occurs concommitantly with uplift. Horizontal velocities at the free surface are zero at the symmetric centerline and increase to ~1 km/10 m.y. at distances of 90-150 km from the rift. The horizontal velocities at the crust mantle interface are 5-10% higher than surface velocities indicating crustal shear. The assumptions of a continuum crust, high crustal viscosities, and a zero horizontal velocity on the left boundary provide spreading rates ~ equal to uplift rates.

Two-dimensional cross sections of the steady-state velocity field as a function of increasing surface heat flow are shown in Figure 9. The

instantaneous velocity vectors of the lithosphere (Z<100 km) are small (V<0.05 mm/yr) whereas the velocities in the asthenosphere beneath the rift (V~1 mm/yr) are large. These cross sections illustrate the shape of the velocity flow field where hot, buoyant asthenosphere flows laterally towards the center of the rift, ascends vertically and spreads outward beneath the lithosphere. As heat transport and surface heat flow increase, the velocity function of the hot buoyant mantle diapir increases by a factor of 10 as shown in Figure 7, the half flow field narrows from >175 km to ~100 km as shown in Figure 8, a marked temperature increase occurs in the lithosphere beneath the rift, and transverse shear increases between lithosphere and asthenosphere. The actual hot, buoyant mantle diapir is ~200 km wide at depths of 200-300 km, increases its width to 300-400 km at the lithosphere-asthenosphere boundary, thins the lithosphere, and creates broad crustal upwarp associated with major continental rifts. In effect, the buoyant process narrows and concentrates heat transport beneath the rift, increases upward velocity, arches the lithosphere, and generates broad surface swells, a well known characteristic of continental rifts since Gregory (1921) defined the structure and surface features of African rifts.

The a priori choice of a 400 km deep model provides a local rather than global solution to mantle convection This local solution does predict uplift rates and mantle viscosities which are in accord with geological data and rebound studies of viscosity (Cathles, 1975; Hager and O'Connell, 1979). The viscosity structure is discussed in a following section. Recent stud indicate convection may be confined to a series of superimposed layers (Richter, 1979). If convection occurs at all depths but is confined to discrete layers such as upper mantle (/ < 670 km) and

lower mantle (670 < Z < 2,900 km), our local model is consistent with convection theory.

Creep coefficients A, E*, V*, and n from Eq. 2 have a range of behavior depending on $\dot{\epsilon}$, T, and material (Carter, 1976). In general, as E* and V* increase, the viscosity increases and velocities decrease (both in a °non-linear fashion). The parameter linearly scales the viscosity (Eq. 2). The free surface velocities are determined by the viscous creep of Eq. 2. For the quasi-elastic crust, n is assumed to be 1, V*=0, whereas A and E* are scaled to produce a viscosity. This viscosity is actually unknown - its value controls surface uplift and hence if we can predict free surface velocities, a constraint has been placed on crustal viscosities asscciated with rifting. A wide range of material parameters for A, E*, V*, and n was studied for upper mantle materials. An A = 3.4 Kbars^{-n}, n = 3, E* = 110 kcal/mole, and V* = 17 cm^3/mol is used in this study.

The viscosity of the lithosphere and asthenosphere is shown in Figure 9. Figure 9a shows the general character of the two-dimensional viscosity field for continental rift and platform. The increase of temperature at the base of the crust and subsequent increase of surface heat flow from 1.6 to 2.5 HFU produced a decrease in crustal viscosity by a factor of 2 from 7 x 10^{25} to 3.5 x 10^{25} poise (see Figure 9) and an increase in free surface velocity by a factor of 3 from 0.5 to 1.3 km/10 m.y. (see Figure 6). The numerical simulations suggest a crustal viscosity of >10^{25} poise is appropriate. A broad, relatively low viscosity region occurs below the rift in the asthenosphere. A relatively small lateral viscosity variation occurs in the lithosphere, with equivalent variation occurring in the crust. As one progresses away from the rift, viscosity increases and the lithosphere

thickens. Figure 9b shows viscosity minima of $\sim 10^{22}$ poise beneath the rift and $\sim 10^{23}$ poise beneath the platform.

The viscosity structure of the earth has been studied in the past 45 years using post glacial rebound data, non-tidal, secular angular acceleration of the earth, polar wandering, and microscopic mechanisms of flow in solids by a host of researchers. The notable studies of Cathles (1975), Peltier (1976), and Hager and O'Connell (1979) review the viscous nature of the solid earth. Present evidence is consistent with a mantle with viscosity on the order of 10^{22} poise overlain by a low viscosity layer of undetermined thickness and viscosity (Hager and O'Connell, 1979). It is likely that mantle viscosities are 1-2 orders of magnitude lower under oceanic and tectonically active continents than under shields. The global kinematic study of large scale mantle flow of Hager and O'Connell (1979) found that the predicted dip of flow for subduction zones agreed best with seismic dip using the following model. A Newtonian viscosity of 10^{25} poise, extending to depths of 64 km, overlies a thin low viscosity layer of 4×10^{20} poise. The lower mantle is modeled as a constant viscosity 10^{22} poise. This model is similar to that of Cathles (1975). Note that the viscosity models of Figure 9 are similar, e.g. a lithosphere of $\sim 10^{25}$ poise overlying an asthenosphere of $\sim 10^{23}$ poise with a tectonically active continental rift having a viscosity of 10^{22} poise.

A tenuous trail is available to explain initial convection of mass and heat into the lithosphere. The rate of rift volcanism, a surface expression of deep seated convection, is small during Oligocene to late Miocene time (40-20 m.y. ago). A sharp increase in rift volcanism occurred following the Miocene lull 17-13 m.y. ago, indicating a major change in crustal magmatism and implying convective sources of heat in the lower

lithosphere and rapidly increasing temperatures at the base of the crust (see Figure 2c). If the proto-rift region had a nearly continental geotherm and average surface heat flow (~1.4 HFU), prior to the Miocene lull its viscosity would have been greater than shown in Figure 9 resulting in a smaller free surface velocity. Hence uplift might have been small. Convective heat transfer following the lull could have increased crustal temperature, decreased mantle and crustal viscosities, and increased surface velocities to values of 1 km/10 m.y. Free surface velocities of 1-1.5 km/10 m.y. for present surface heat flow of 2.5 HFU and crustal temperatures of ~1000°C satisfy geologic evidence for uplift. Regional uplift of 1-1.5 km produced present topography of ~2 km (see Figure 1); uplift began ~10-15 m.y. ago based on paleobotanical evidence and block faulting. Recall though, that this is a tradeoff because crustal viscosities are unknown. If crustal viscosities are larger (e.g. 2×10^{26} poise) free surface velocities are smaller (e.g. 0.1-0.5 km/10 m.y.) and regional uplift would take 30 m.y. for present temperature and heat flow. Figure 10 shows a comparison of measured, regionally averaged, and calculated topography for the Rio Grande rift.

CONCLUSIONS

Present geologic features of the Rio Grande rift include regional topography >2 km, surface heat flow of >2.5 HFU, a geotherm with gradient >30°C/km, temperatures at the base of the crust of ~1000°C, and an increase in rift volcanism in late Miocene time. Geologic constraints on rate of uplift, based on inception of block faulting and paleobotanical evidence, suggest this uplift was initiated 10-15 m.y. ago on a broad regional scale. A concurrent outpouring of volcanics occurred over a large portion of the

rift. These geologic data are used to provide constraints for the many unknowns of the thermomechanical problem. A suite of thermal profiles is evaluated to describe the viscosity structure, velocity profiles, and uplift of the rift.

Temperatures at the base of the crust have the range $600 < T < 1000°C$ for continent and rift. The crustal viscosity, which provides final uplift velocities of 1.3 km/10 m.y. at a surface heat flow of 2.5 HFU, is $C \times 10^{25}$ poise. The coefficients of the Weertman creep law, Eq. 2, which provide reasonable flow velocities of upper mantle and viscosities of $10^{22} - 10^{23}$ poise, are $A = 3.4$ kbar^{-n} $E^* = 110$ kcal/mol, $V^* = 17$ cm^3/mol, and $n = 3$. The steady-state creep field has a zone of flow toward the rift at asthenospheric depths of >325 km, a region of hot, buoyant uplift ~150-200 km wide between 200 and 300 km depth, and an outward spreading lobe ~300-400 km wide in the upper asthenosphere beneath the rift. Free surface velocities range from 0.5 to 1.5 km/10 m.y. as heat flow increases from 1.6 to 2.5 HFU for the relatively stiff, viscous lithosphere. Vertical velocity profiles through the mantle diapir increase from 1.8 km/10 m.y. beneath the cold continent to 1.2 km/m.y. in the buoyant mantle diapir beneath the rift, a factor of ~10. Horizontal spreading velocities are ~1 km/10 m.y. to provide spreading rates approximately the same as uplift rates. The rift process narrows and concentrates heat transport beneath the rift, increases upward velocity, and broadly arches the lithosphere. Calculated topography reaches a maximum value of 2 km at the continental rift and diminishes in accord with measured topography towards the continental platform.

The crust, acting as a elastic/highly viscous body, and the relatively cold upper mantle, which together comprise the lithosphere, exhibit a profound effect on thermomechanical processes of continental rifting. This 'cap' damps out convective motion, aids in broadly spreading uplift because of shear tractions at its base, absorbs vast quantities of heat, and resists brittle deformation. Flow in the underlying asthenosphere becomes decoupled through the increase in velocity and sharp reduction in viscosity.

ACKNOWLEDGMENTS

The early interaction and support of Tom McGetchin, and his incessant good cheer, started the initial chain of events leading to this paper. Many discussions with K. Bailey, S. Baldridge, J. Callender, C. Chapin, R. Girdler, R. Keller, P. Mohr, G. Palmason, I. Ramberg, B. Seager, and T. Shankland have benefitted the evolving ideas of rift processes. W. S. Baldridge and T. J. Shankland provided critical reviews.

SELECTED REFERENCES

Aiken, C. L. V., A. W. Laughlin, and F. G. West, Residual Bouguer Gravity Map of New Mexico. Los Alamos Scientific Laboratory Report, LA-7466-MAP, August 1978.

Anderson, C. and R. J. Bridwell, A Finite Element Creep Method for Studying the Transient Nonlinear Thermal Creep of Geological Structures, in press, Int. Jour. Num. and Analy. Methods in Geomechanics, 1980.

Axelrod, D. I. and H. P. Bailey, Tertiary Vegetation, Climate, and Altitude of the Rio Grande Depression, New Mexico - Colorado, Paleobiology, 2, 235-254, 1976.

Baldridge, W. S., P. E. Damon, M. Shafiqullah, and R. J. Bridwell, New Potassium-Argon Ages: Evolution of the Central Rio Grande Rift, New Mexico, manuscript in prep., 1980.

Blackwell, D. D., The Thermal Structure of the Continental Crust, in Hancock, J. G., ed.: Am. Geophys. Un. Monograph 14, 169-184, 1971.

Bridwell, R. J., Lithospheric Thinning and the Late Cenozoic Thermal and Tectonic Regime of the Northern Rio Grande Rift, New Mexico Geol. Soc. Guidebook, 27th Field Conf., Vermejo Park, 283-292, 1976.

Bridwell, R. J., The Rio Grande Rift and a Diapiric Mechanism for Continental Rifting, in Tectonics and Geophysics of Continental Rifts, Proc. NATO Adv. Study Inst. on Paleorift Systems with Emphasis on Permian Oslo Rift, Ramberg and Neumann eds., Reidel, Boston, 2, 73-80, 1978a.

Bridwell, R. J., Physical Behavior of Upper Mantle Beneath Northern Rio Grande Rift, in Guidebook to Rio Grande Rift in New Mexico and Colorado, J. W. Hawley, ed., NM Bur. Mines and Min. Res., Circ. 163, 228-230, 1978b.

Bridwell, R. J. and C. A. Anderson, Dynamic Thermomechanical Structure of Continental Rifts, Manusc. in prep for Continental and Oceanic Rifts, Geophys. Un. Geodynamics Series (1980).

Jles, L. M., III, The Viscosity of the Earth's Mantle, Princeton University Press, Princeton, NJ, 1975.

Carter, N. L., Steady State Flow of Rocks, Res. Geophys. and Space Phys., 14, 301-360, 1975.

Chapin, C. E. and W. Seager, Evolution of the Rio Grande Rift in the Socorro and Las Cruces Areas, New Mexico Geol. Soc. Guidebook, 26th Field Conf., 297-322, 1975.

Cook, F. A., D. B. McCullar, E. R. Decker, and S. B. Smithson, Crustal Structure and Evolution of the Southern Rio Grande Rift, in Rio Grande Rift: Tectonics and magmatism, Riecker, ed., Am. Geophys. Un. Spec. Pub., 195-208, 1979.

Decker, E. R. and S. B. Smithson, Heat Flow and Gravity Interpretation Across the Rio Grande Rift in Southern New Mexico and West Texas, J. Geophys. Res., 80, 2542-2552, 1975.

Epis, R. C. and C. E. Chapin, Geomorphic and Tectonic Implications of the Post-Laramide, Late Eocene Erosion Surface in the Southern Rocky Mountains, in Cenozoic History of Southern Rocky Mountains, Geol. Soc. Mem. 148, 45-74, 1975.

Froidevaux, C. and G. Schubert, Plate Motion and Structure of the Continental Asthenosphere: A Realistic Model of the Upper Mantle, J. Geophys. Res., 80, 2553-2564, 1975.

Gregory, J. W., Rift Valleys and Geology of East Africa, Seclay Service, London, 479 pp., 1921.

Hager, B. R. and R. J. O'Connell, Kinematic Models of Large-Scale Flow in the Earth's Mantle, J. Geophys. Res., 84, 1031-1048, 1979.

Lubimova, E. A., Heat Flow Pattern in Baikal and Other Rift Zones, Tectonophysics, 8, 457-468, 1969.

McGetchin, T. R. and L. T. Silver, Compositional Relations in Minerals from Kimberlite and Related Rocks in the Moses Rock Dike, San Juan County, Utah, Amer. Mineral., 55, 1738-1771, 1972.

Mercier, J-C. C., Natural Peridotites;; Chemical and Rheological Heterogeneity of the Upper Mantle, Ph.D. Thesis, SUNY, Stonybrook, 1977.

Olsen, K. H., G. R. Keller, and J. N. Stewart, Crustal Structure Along the Rio Grande Rift from Seismic Refraction Profiles, in Rio Grande Rift: Tectonics and Magmatism, R. E. Riecker, ed., Am. Geophys. Union Spec. Pub., 127-144, 1979.

Padovani, E. R. and J. L. Carter, Aspects of the Deep Crustal Evolution Beneath South Central New Mexico, in The Earth's Crust, Geophys. Monogr. Ser., Vol. 20, edited by J. G. Heacock, AGU, Washington, DC, 1977.

Peltier, W. R., Glacial Isostatic Adjustment II, The Inverse Problem, Geophys. J. Roy. Astron. Soc., 46, 669-706, 1976.

Prager, W., Introduction to Mechanics of Continua, Ginn & Co., 154-157, 1961.

Ramberg, I. B., Cook, F. A., and S. B. Smithson, Structure of the Rio Grande Rift in Southern New Mexico and West Texas Based on Gravity Interpretation, Geol. Soc. Amer. Bull., 89, 107-123, 1978.

Reiter, M., C. L. Edwards, H. Hartman, and C. Weidman, Terrestrial Heat Flow Along the Rio Grande Rift, New Mexico and Southern Colorado, Geol. Soc. Amer. Bull., 86, 811-818, 1975.

Ross, J. V., H. G. Ave' Lallemant, and N. L. Carter, Activation Volume for Creep in the Upper Mantle, Sci., 203 (9), 261-263, 1979.

Schatz, J. F. and M. G. Simmons, Thermal Conductivity of Earth Material at High Temperatures, Jour. Geophys. Res., 77, 6966-6783, 1972.

Schubert, G. and D. L. Turcotte, One-Dimensional Model of Shallow Mantle Convection, J. Geophys. Res., 77, 945-951, 1972.

Schubert, G., C. Froidevaux, and D. A. Yuen, Oceanic Lithosphere and Asthenosphere: Thermal and Mechanical Structure, J. Geophys. Res., 81, 3525-3540, 1976.

Schubert, G., D. A. Yuen, C. Froidevaux, L. Fleitout, and M. Sourian, Mantle Circulation with Partial Shallow Return Flow: Effects on Stresses in Oceanic Plates and Topography of the Sea Floor, J. Geophys. Res., 83, 745-758, 1978.

Skinner, B. J., Thermal Expansion, Handbook of Physical Constants, Geol. Soc. Amer. Mem., 97, 75-96, 1966.

Richter, F. M., Focal Mechanisms and Seismic Energy Release of Deep and Intermediate Earthquakes in the Tonga - Kermadec Region and Their Bearing on the Depth Extent of Mantle Flow, J. Geophys. Res., 84, 6783-6795, 1979.

FIGURE CAPTIONS

Figure 1. Regional topography of New Mexico. The Rio Grande rift is outlined by the hachured region. Contour interval in feet. Modified from Aiken et al. 1978.

Figure 2. Cenozoic volcanism, tectonic evolution, and schematic thermal history of Rio Grande rift. (a) 161 K/Ar and fission track dates from Chapin and Seager, 1975. (b) Tectonic evolution of Rio Grande rift north of Socorro, New Mexico. (c) Postulated thermal pulse associated with rifting in New Mexico. The pre-Miocene-lull thermal pulse is schematic because most of the data set represents age dates from the Datil-Mogollon volcanic field.

Figure 3. Continental rift and platform geotherms. The continental platform geotherm is shown as a heavy dashed line (McGetchin and Silver, 1972). The continental rift geotherm is shown as a heavy stippled line. The remaining solid lines are extrapolated to temperatures of the olivine-spinel phase transition. Numbers in parentheses above the rift geotherm represent gradients in °C/km. Numbers at Moho depths represent the surface heat flow in heat flow units (HFU).

Figure 4. Schematic diagram of thermomechanical model, constraints, and unknowns for numerical calculations of rifting.

Figure 5. Temperature profiles beneath a continental rift and platform. The notation of increase in surface heat flow from 1.6 to 2.5 HFU is shown on the top left boundary of the model. Note increasingly higher temperatures at shallow depths. These cases are shown in profile from Figure 3.

Figure 6. Plot of free surface velocities as a function of time for surface heat flow $1.6 < q_s < 2.5$ HFU. Velocity profiles occur on symmetric centerline of model.

Figure 7. Steady-state velocity profile as a function of depth, the lithosphere and asthenosphere for continental rift. This figure is a snapshot of the instantaneous velocity field for $t \sim 15$ m.y. as q_s ranges from 1.6 to 2.5 HFU. A priori, the base of the lithosphere is that change in slope where the velocity increases markedly. Note that there is little change where $q_s \sim 1.6$ HFU whereas the increase in heat transport thins the lithosphere as $q_s \sim 2.5$ HFU.

Figure 8. Two-dimensional steady-state velocity flow fields as heat transport increases beneath Rio Grande rift. Successive snapshots of the instantaneous flow field at t ≈15 m.y. show the growth of the hot, buoyant mantle diapir beneath a continental rift.

Figure 9. Viscosity of a continental rift and platform.
a. Two-dimensional variation of viscosity for present surface heat flow of Rio Grande rift.
b. Range of viscosity and minima as temperature increases at base of crust beneath rift.

Figure 10. Comparison of surface, regional, and calculated topography. Surface heat flow for Baikal and Rio Grande rifts are also shown.

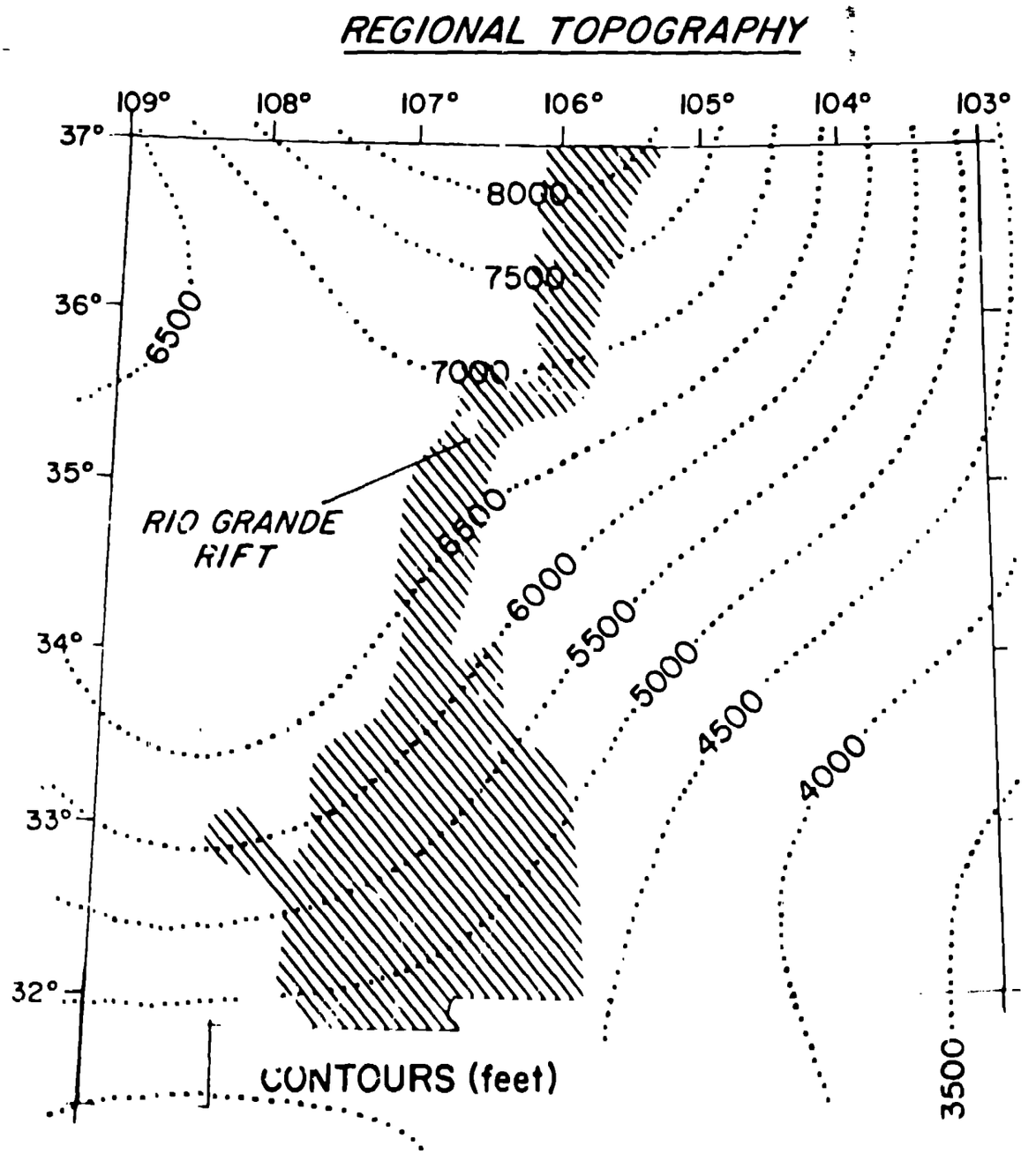
REGIONAL TOPOGRAPHY
109°
108°
107°
106°
105°
104°
103°
37°
36°
35°
34°
33°
32°
8000
7500
7000
6500
6000
5500
5000
4500
4000
3500
RIO GRANDE RIFT
CONTOURS (feet)

Fig. 1

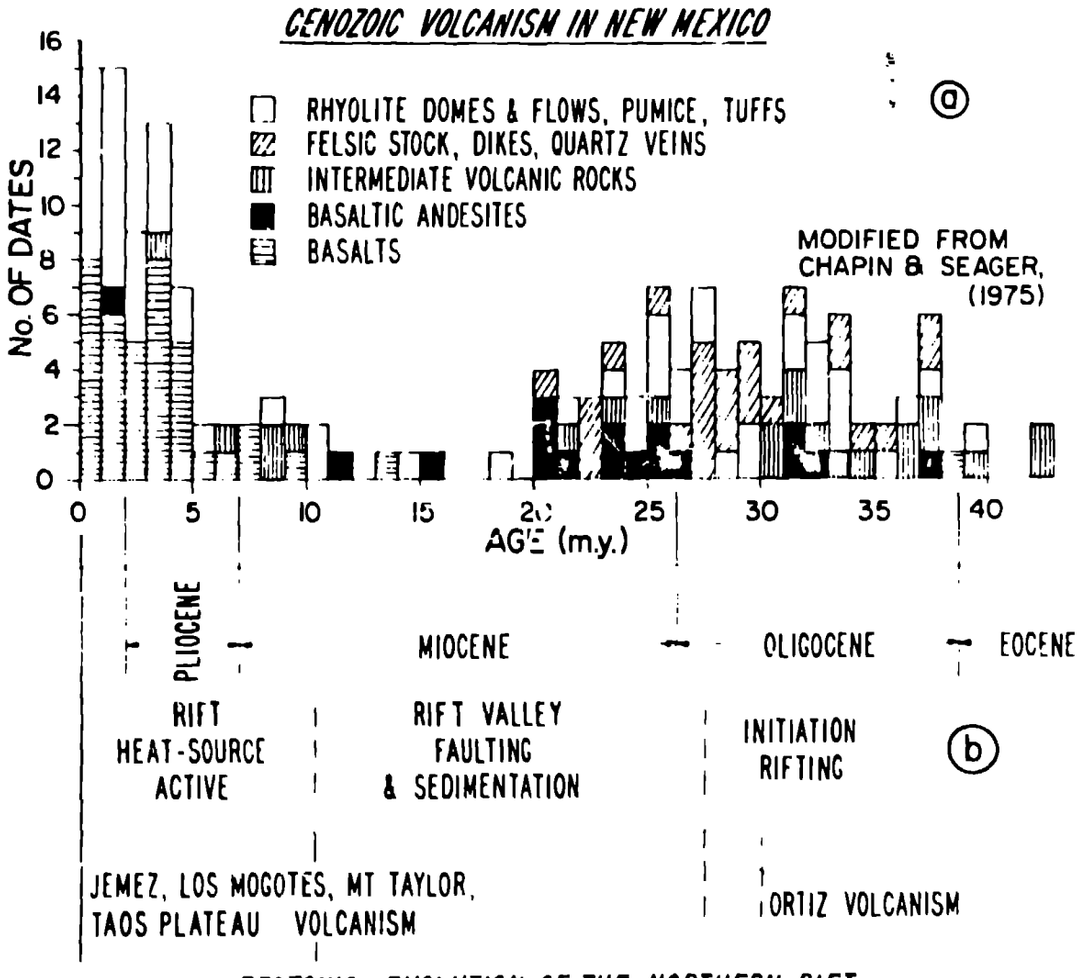
CENOZOIC VOLCANISM IN NEW MEXICO
RHYOLITE DOMES & FLOWS, PUMICE, TUFFS
FELSIC STOCK, DIKES, QUARTZ VEINS
INTERMEDIATE VOLCANIC ROCKS
BASALTIC ANDESITES
BASALTS
MODIFIED FROM CHAPIN & SEAGER, (1975)
No. OF DATES
AGE (m.y.)
PLIOCENE
MIOCENE
OLIGOCENE
EOCENE
RIFT HEAT-SOURCE ACTIVE
RIFT VALLEY FAULTING & SEDIMENTATION
INITIATION RIFTING
JEMEZ, LOS MOGOTES, MT TAYLOR, TAOS PLATEAU VOLCANISM
ORTIZ VOLCANISM
TECTONIC EVOLUTION OF THE NORTHERN RIFT

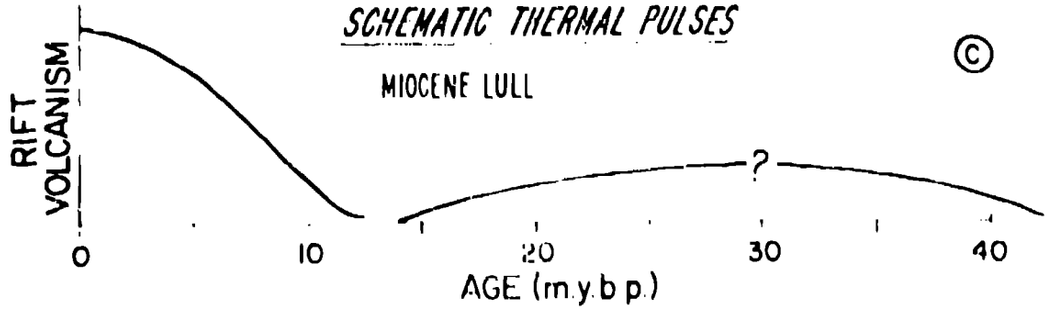
SCHEMATIC THERMAL PULSES
MIOCENE LULL
RIFT VOLCANISM
AGE (m.y.b.p.)

Fig. 2

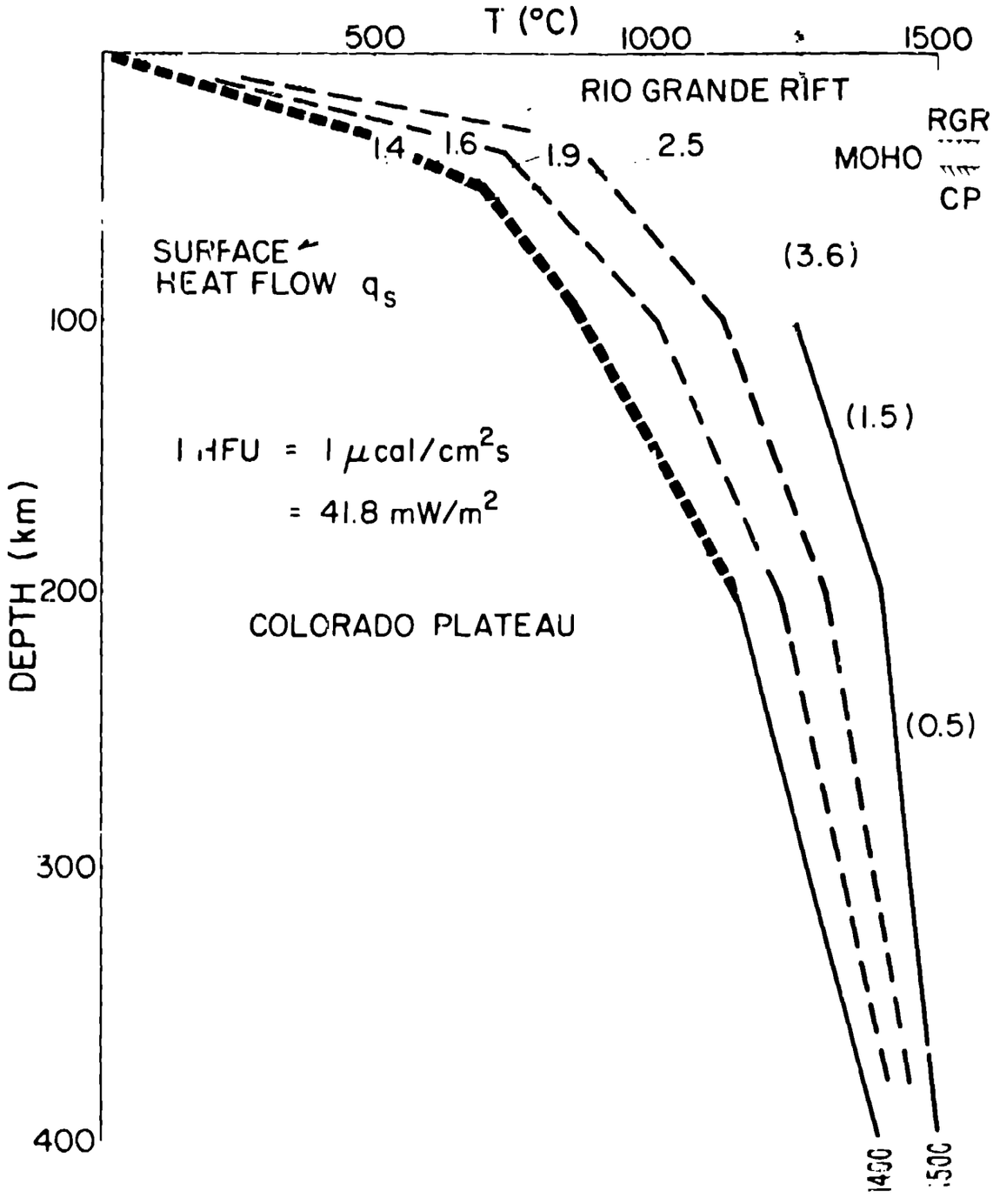
T (°C)
500
1000
1500
RIO GRANDE RIFT
RGR
MOHO
CP
1.4
1.6
1.9
2.5
(3.6)
(1.5)
(0.5)
SURFACE
HEAT FLOW q_s
1 HFU = 1 μcal/cm^{2}s
= 41.8 mW/m^2
COLORADO PLATEAU
DEPTH (km)
100
200
300
400
1400
1500

Fig. 3

GEOMETRY and BOUNDARY CONDITIONS

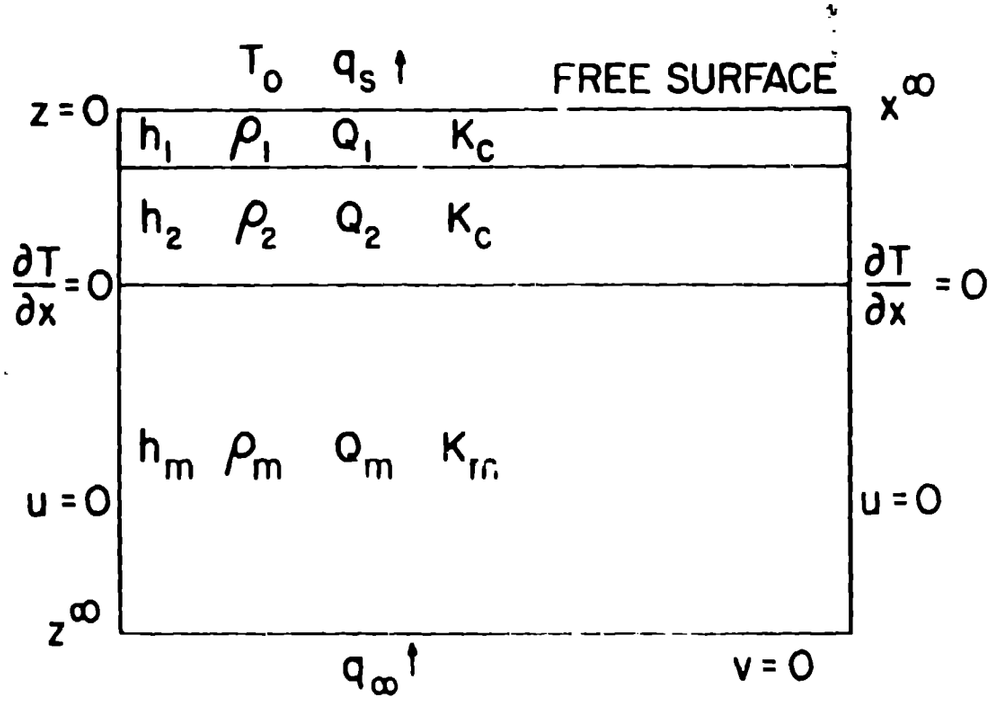

BOUNDARY CONDITIONS

$T = T_0$ FREE SURFACE at $z = 0$

$q = q_\infty$ $v = 0$ at z^∞

$\frac{\partial T}{\partial x} = 0$ $u = 0$ at $x = 0, x^\infty$

UNKNOWNS

$T(z)$ GEOTHERM

τ EFFECTIVE STRESS

η EFFECTIVE VISCOSITY

u, v VELOCITIES IN x & z DIRECTIONS

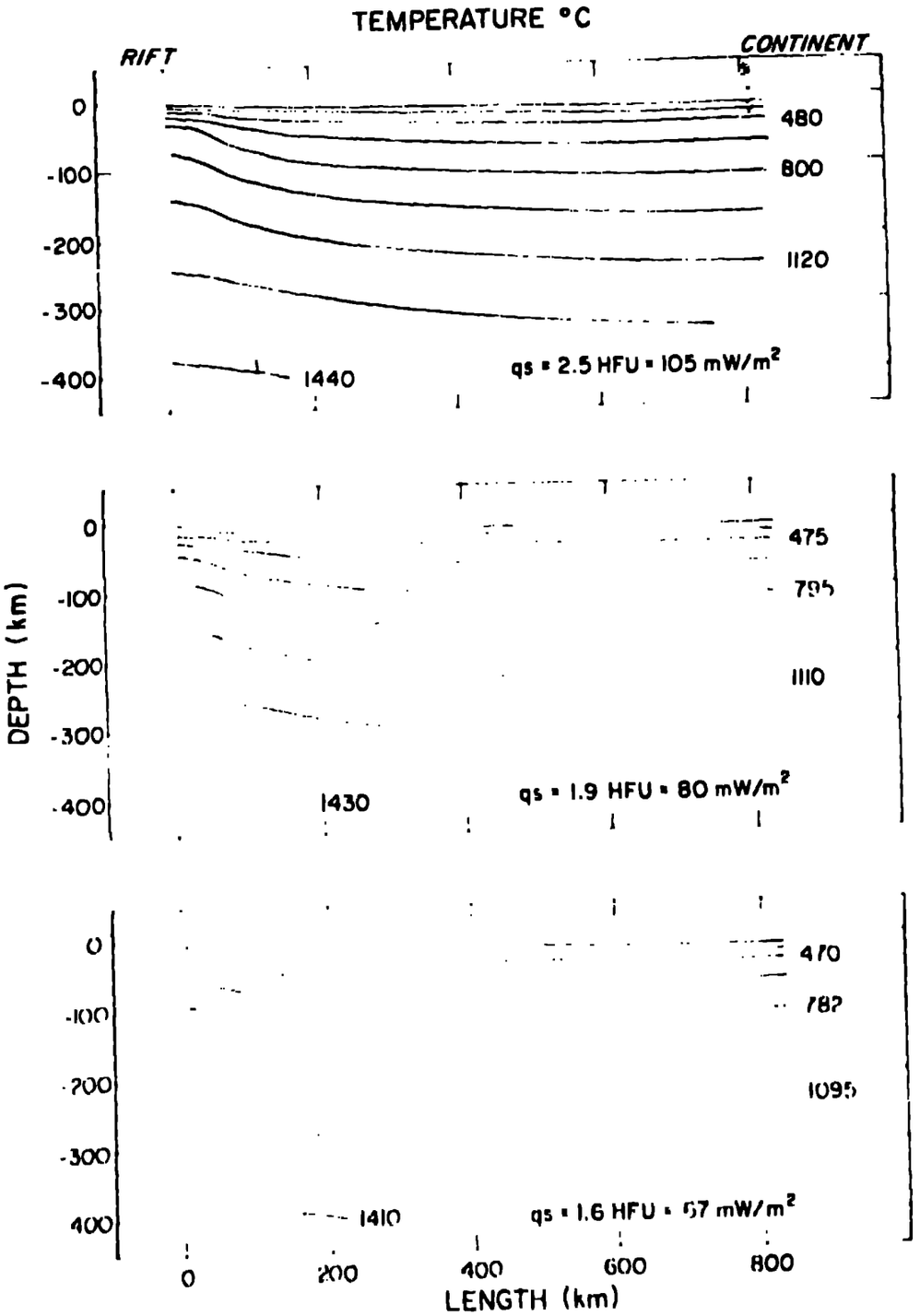
TEMPERATURE °C
RIFT
CONTINENT
0
-100
-200
-300
-400
480
800
1120
1440
qs = 2.5 HFU = 105 mW/m²
DEPTH (km)
475
795
1110
1430
qs = 1.9 HFU = 80 mW/m²
470
782
1095
1410
qs = 1.6 HFU = 67 mW/m²
0
200
400
600
800
LENGTH (km)

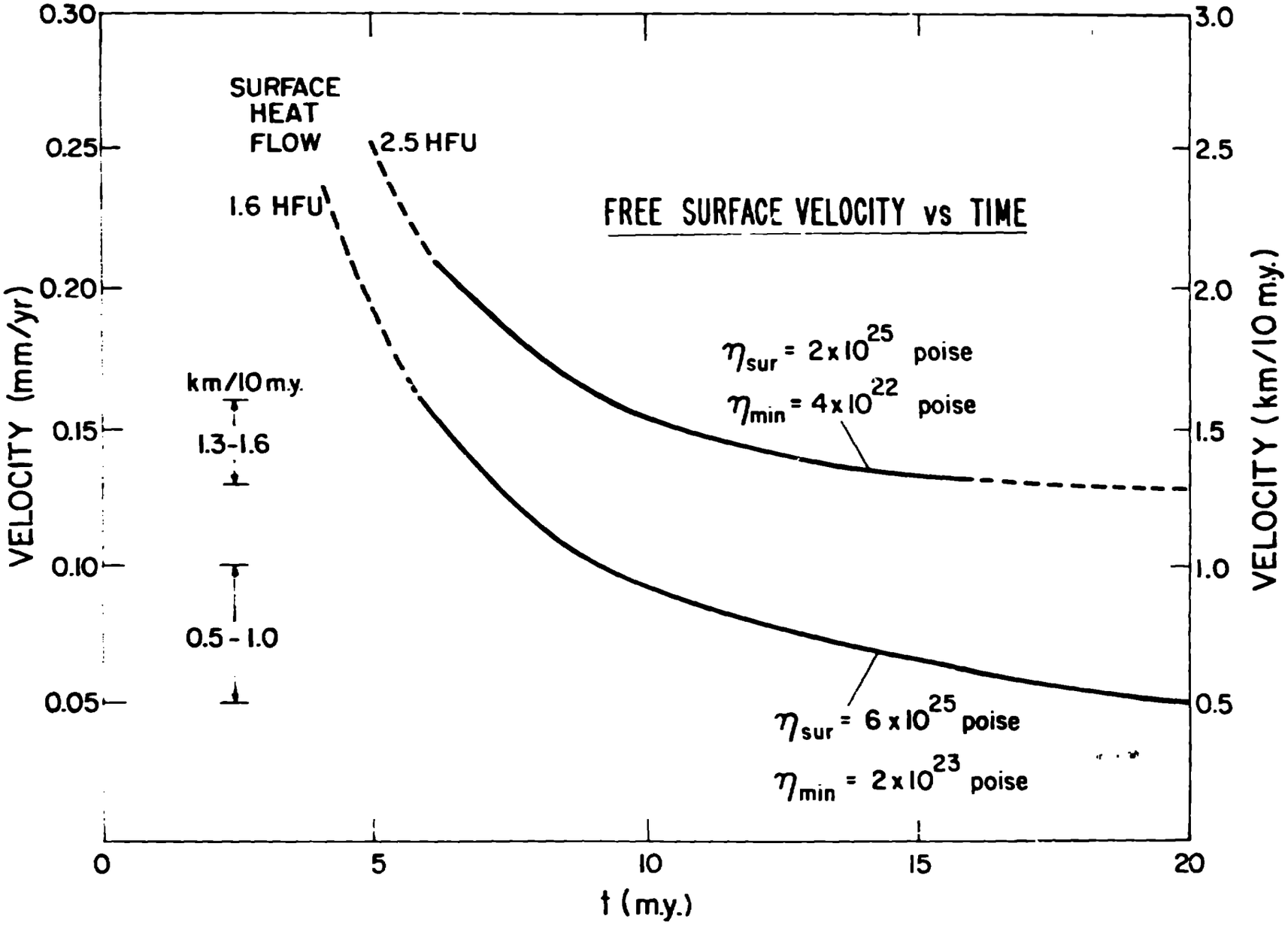
FREE SURFACE VELOCITY vs TIME
SURFACE HEAT FLOW
2.5 HFU
1.6 HFU
km/10 m.y.
1.3-1.6
0.5 - 1.0
η_{sur} = 2 x 10^25 poise
η_{min} = 4 x 10^22 poise
η_{sur} = 6 x 10^25 poise
η_{min} = 2 x 10^23 poise
VELOCITY (mm/yr)
VELOCITY (km/10 m.y.)
t (m.y.)
0.30
0.25
0.20
0.15
0.10
0.05
3.0
2.5
2.0
1.5
1.0
0.5
0
5
10
15
20

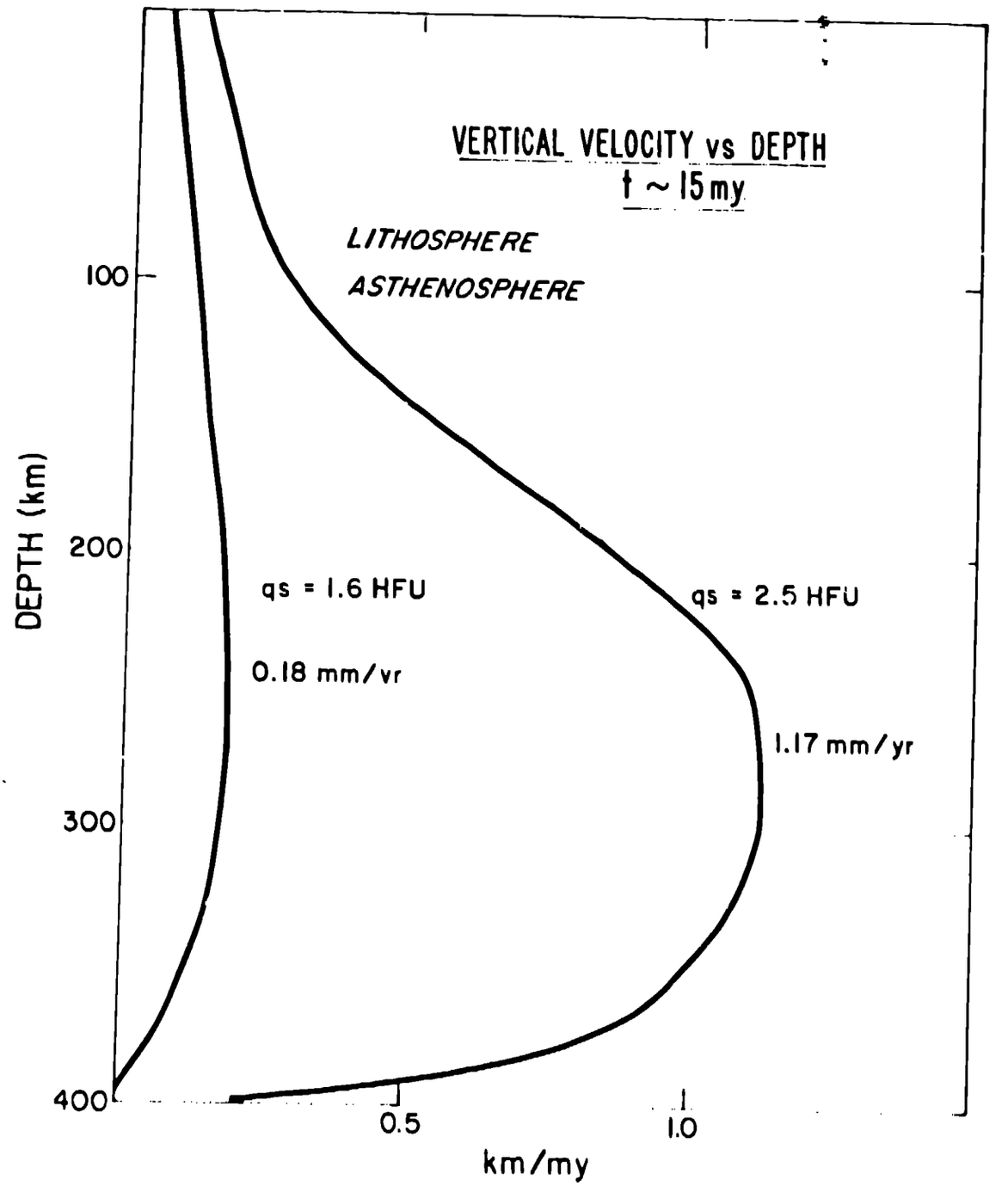
VERTICAL VELOCITY vs DEPTH
t ~ 15 my
LITHOSPHERE
ASTHENOSPHERE
DEPTH (km)
100
200
300
400
qs = 1.6 HFU
0.18 mm/yr
qs = 2.5 HFU
1.17 mm/yr
0.5
1.0
km/my

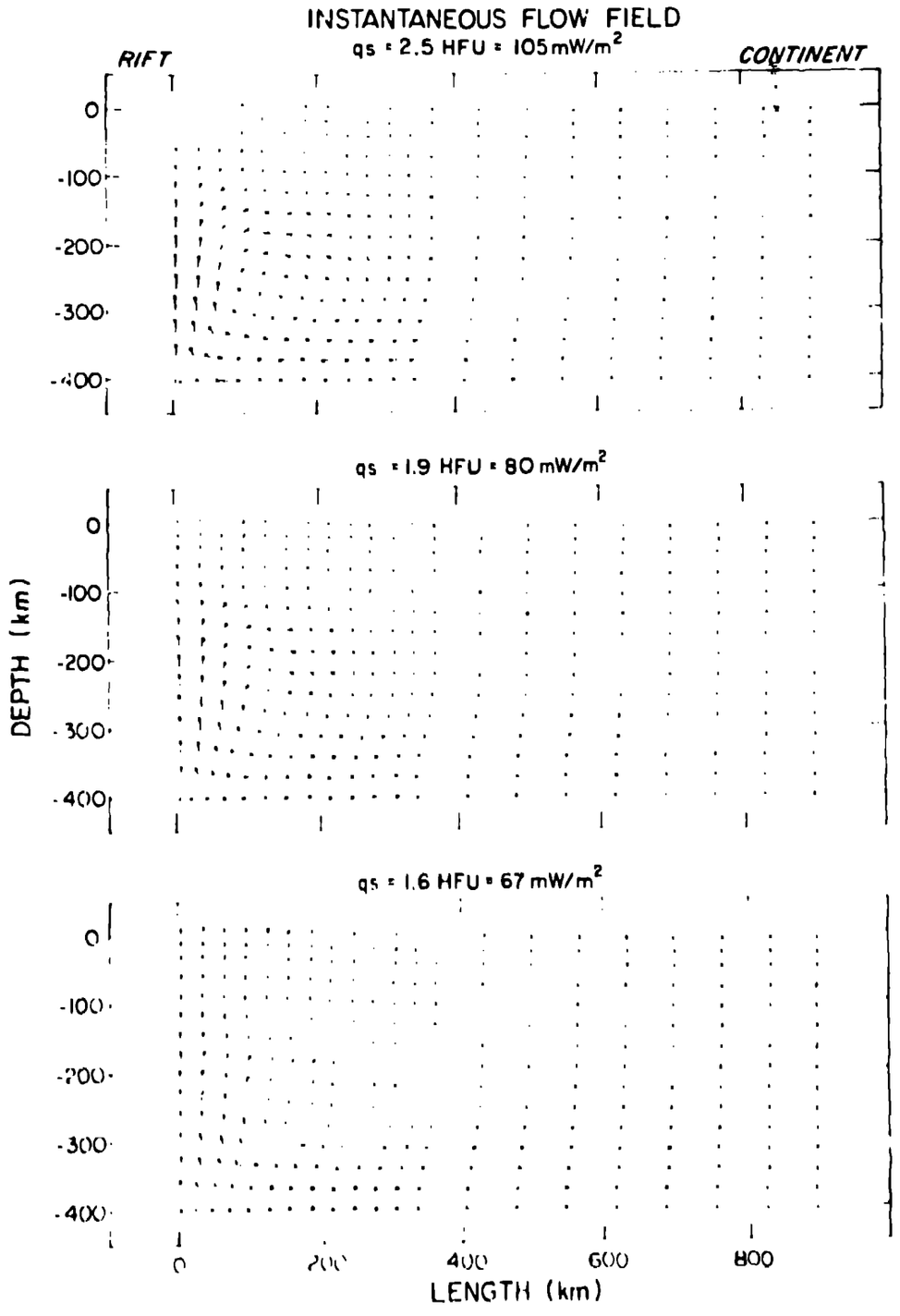
INSTANTANEOUS FLOW FIELD
qs = 2.5 HFU = 105 mW/m²
RIFT
CONTINENT
0
-100
-200
-300
-400
qs = 1.9 HFU = 80 mW/m²
qs = 1.6 HFU = 67 mW/m²
DEPTH (km)
0
400
600
800
LENGTH (km)

Fig. 8

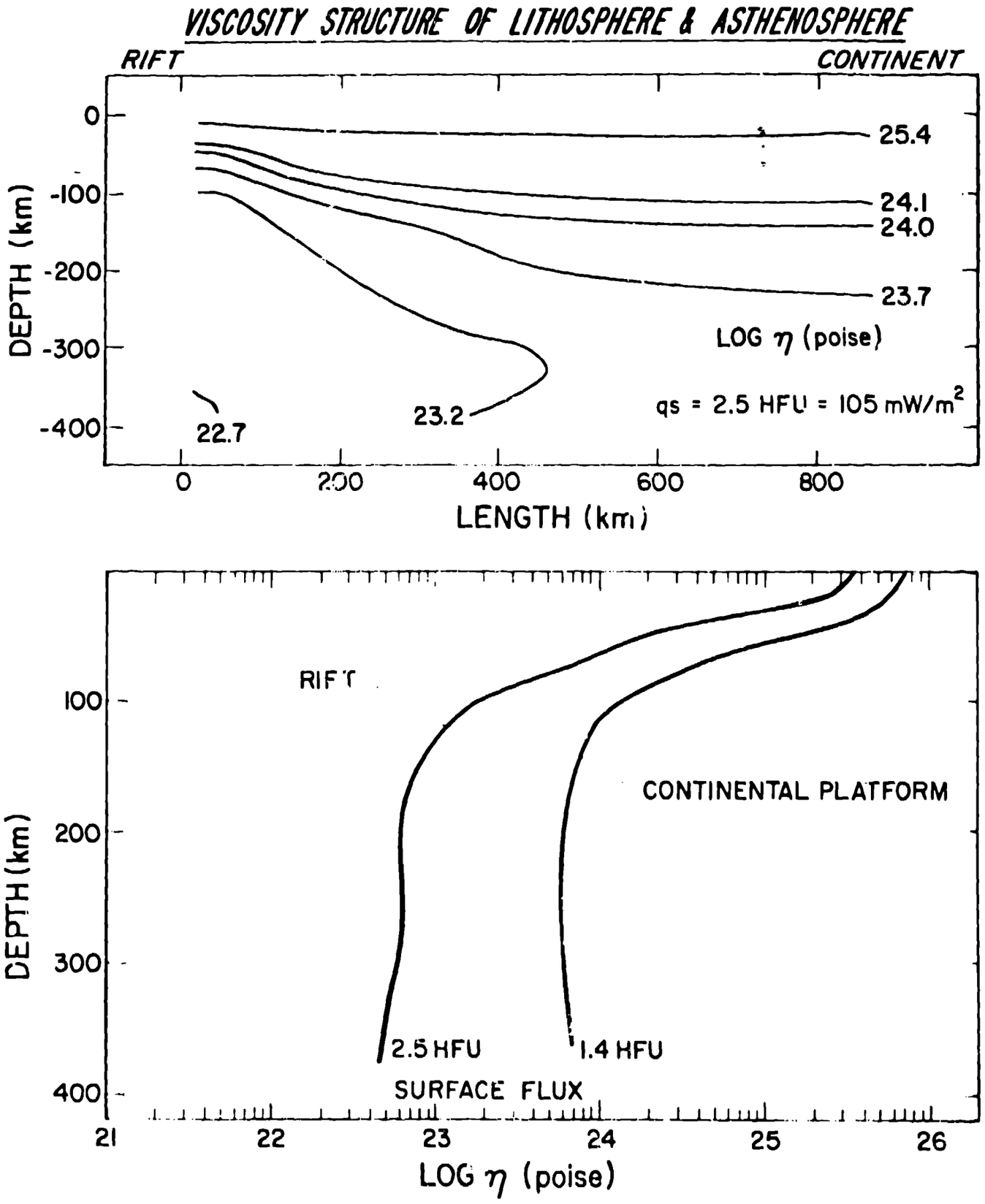
VISCOSITY STRUCTURE OF LITHOSPHERE & ASTHENOSPHERE
RIFT
CONTINENT
0
-100
-200
-300
-400
DEPTH (km)
25.4
24.1
24.0
23.7
LOG η (poise)
qs = 2.5 HFU = 105 mW/m²
23.2
22.7
0
200
400
600
800
LENGTH (km)
RIFT
CONTINENTAL PLATFORM
100
200
300
400
DEPTH (km)
2.5 HFU
1.4 HFU
SURFACE FLUX
21
22
23
24
25
26
LOG η (poise)

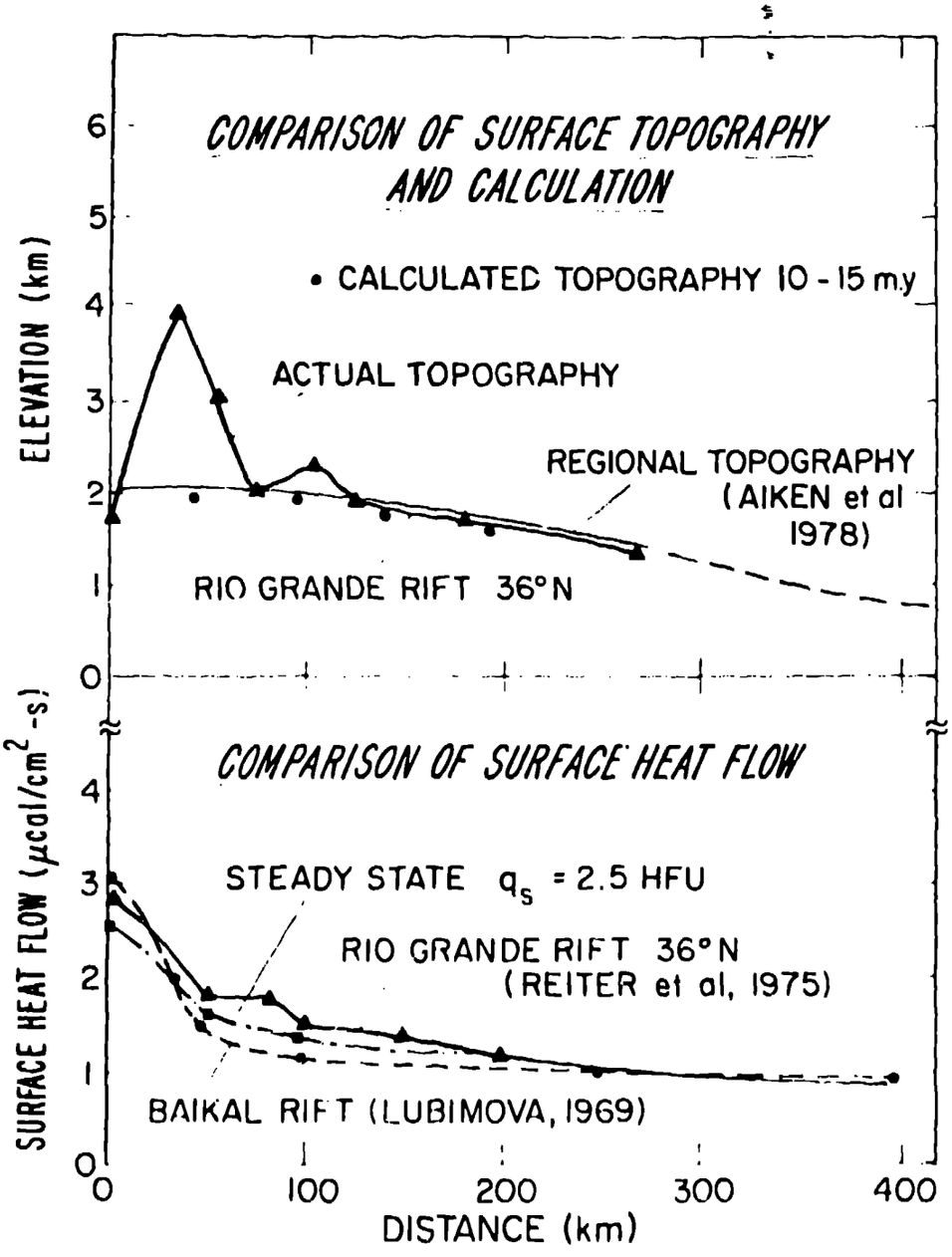
COMPARISON OF SURFACE TOPOGRAPHY AND CALCULATION
• CALCULATED TOPOGRAPHY 10 - 15 my
ACTUAL TOPOGRAPHY
REGIONAL TOPOGRAPHY (AIKEN et al 1978)
RIO GRANDE RIFT 36°N
ELEVATION (km)
COMPARISON OF SURFACE HEAT FLOW
STEADY STATE q_s = 2.5 HFU
RIO GRANDE RIFT 36°N (REITER et al, 1975)
BAIKAL RIFT (LUBIMOVA, 1969)
SURFACE HEAT FLOW (μcal/cm^2-s)
DISTANCE (km)